Structural basis of novel bile acid-based modulators of FXR

Kydd-Sinclair, D. ORCID: https://orcid.org/0000-0002-5423-537X, Packer, G. L., Weymouth-Wilson, A. C. and Watson, K. A. ORCID: https://orcid.org/0000-0002-9987-8539 (2025) Structural basis of novel bile acid-based modulators of FXR. Journal of Molecular Biology, 437 (21). 169383. ISSN 0022-2836 doi: 10.1016/j.jmb.2025.169383 Available at https://centaur.reading.ac.uk/124155/

Research Article

Structural Basis of Novel Bile Acid-Based Modulators of FXR

D. Kydd-Sinclair [1,*], G. L. Packer [2], A. C. Weymouth-Wilson [2,3], and K. A. Watson [1,*]

*1 - **School of Biological Sciences,** Health and Life Sciences Building, Whiteknights Campus, University of Reading, Reading, Berkshire RG6 6EX, UK*
*2 - **NZP UK Ltd,** Thames Valley Science Park, The Gateway, 1 Collegiate Square, Reading, Berkshire RG2 9LH, UK*
*3 - **ICE Group,** Via Sicilia 8/10, 42122 Reggio Emilia, Italy*

***Correspondence to D. Kydd-Sinclair and K.A. Watson:** dannielle.kydd-sinclair@reading.ac.uk (D. Kydd-Sinclair), k.a.watson@reading.ac.uk (K.A. Watson)*
https://doi.org/10.1016/j.jmb.2025.169383
Edited by Sepideh Khorasanizadeh

Abstract

Following its deorphanisation in the early 2000s, the farnesoid X receptor (FXR) attracted significant attention for regulating genes involved in bile acid, lipid and glucose metabolism and inflammation, pathways central to many liver diseases. As such, pharmaceutical efforts targeted FXR for their treatment. However, while FXR agonists, such as obeticholic acid, have been studied in clinical trials, many were associated with adverse effects arising from the promiscuity of systemic FXR activation, thus efforts to limit or selectively modulate the downstream effects of FXR are crucially important. In work here, two novel bile acid derivatives, previously identified via molecular docking and cell-based screening, were validated by X-ray crystallography and tested in LanthaScreen coactivator recruitment assays. Their effects on downstream FXR signalling were assessed *in vitro* in hepatocellular carcinoma cells, and *in vivo* in C57BL/6 mice, by RNA sequencing and RT-qPCR. The novel compounds exhibited potent and selective FXR agonist activity. Co-crystal structures of FXR LBD with both compounds, demonstrated distinctive binding modes for each, including occupancy of a receptor sub-pocket associated with allosteric activation, not observed with classic bile acids. Both compounds were up to four-fold more potent than obeticholic acid and demonstrated ligand-dependent differences in coactivator recruitment assays. *In vitro*, both compounds induced greater changes in the expression of FXR target genes, at lower doses than obeticholic acid. I*n vivo*, compound-dependent differential gene expression was observed. These findings suggest that the novel compounds may enable gene-specific FXR regulation through differential coactivator usage and hold potential to overcome the shortcomings of current bile acid drugs, thus representing promising candidates for further research.

Introduction

The Farnesoid X Receptor (FXR, NR1H4) is a member of the nuclear receptor superfamily of ligand-activated transcription factors [1–3]. It is highly expressed in the liver and intestines and is activated by endogenous bile acids. As with other classic nuclear receptors, FXR has a modular architecture and can act independently as a monomer, homodimer, or in conjunction with a heterodimer partner, Retinoid X Receptor (RXR) [4–6]. It is comprised of a largely disordered *N*-terminal region, a DNA binding domain that is responsible for the interactions with specific response elements on its

target genes, and a *C*-terminal ligand binding domain (LBD) that determines the transcriptional activation of the receptor (Figure 1A). The LBD structure comprises 12 alpha helices arranged to form a highly hydrophobic ligand-binding pocket that can discriminate the unique structure of bile acids, as seen in pdb_00001osv and pdb_00001ot7 [5,7,8]. Upon ligand binding, the LBD undergoes a conformational change in which helix 12 is stabilised in a position that promotes the dissociation of corepressor proteins and exposes a hydrophobic interaction surface on helix 3 (Figure 1B). Coactivator protein complexes are subsequently recruited to this site and further induce the recruitment of other transcription factors in a complex process which ultimately initiates the transcription of target genes responsible for FXR's pleiotropic effects [9,10].

FXR is considered the master regulator of bile acid homeostasis [11–13]. When activated, FXR induces fibroblast growth factor 19 (FGF19) in the small intestines and the small heterodimer partner (SHP) in the liver, both of which, via independent mechanisms, act to repress the hepatic expression of the key bile acid synthesis enzyme, cholesterol 7-alpha hydroxylase (CYP7A1) [14,15]. In addition, FXR can upregulate the expression of bile acid transporters such as the bile salt export pump (BSEP) and the organic solute transporter alpha–beta (OSTα/β) to tightly control bile acid circulation and concentrations within hepatocytes [16,17]. Accordingly, extensive research has identified a pivotal, hepatoprotective role of FXR in pathologies such as cholestasis, which is characterised by the overexposure of hepatocytes to toxic bile acids [18,19]. Moreover, FXR regulates genes involved in lipid, cholesterol and glucose metabolism, as well as mechanisms mediating inflammation and fibrosis [20–22]. As such, FXR has been clinically validated as a therapeutic target of metabolic dysfunction-associated steatohepatitis (MASH, previously known as non-alcoholic steatohepatitis), which arises due to the accumulation of lipid intermediates driving hepatocellular injury, inflammation, and fibrosis [23–25].

To date, obeticholic acid (OCA) (Figure 1C) has been the most clinically advanced FXR agonist. It was developed by medicinal chemistry efforts to exploit the scaffold of the most potent naturally occurring bile acid ligand, chenodeoxycholic acid (CDCA), compared with which, it is 100 times

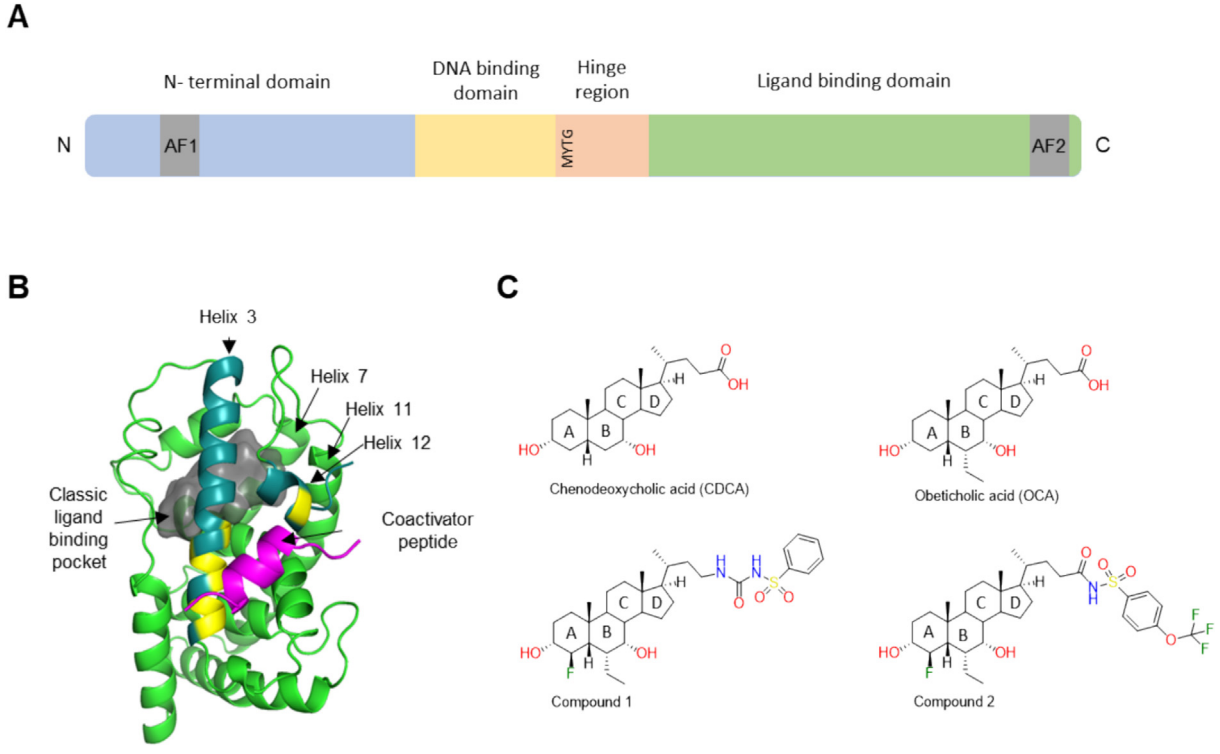

Figure 1. Overall domain architecture and structure of the FXR LBD and steroidal agonists. (**A**) The domain architecture of full length FXR including the N-terminal disordered region, DNA-binding domain and ligand binding domain [21]. (**B**) Alpha helical sandwich structure of the FXR LBD (pdb_00006HL1) showing helices 3 and 12 (both teal) with activation function 2 activity (AF2) directly involved in coactivator (magenta) recruitment site formation and receptor activation. Residues forming coactivator binding cleft are shown in yellow. Classic ligand binding pocket shown as grey surface. (**C**) Structure of the most potent endogenous human bile acid CDCA, semi-synthetic OCA, and two novel bile acid analogue compounds **1** and **2**, with A-D rings labelled.

more potent [26,27]. In randomised control trials (RCTs) assessing the efficacy of OCA in patients with Primary Biliary Cholangitis (PBC), OCA demonstrated promising results and improved clinical endpoints, including significant reductions in alkaline phosphatase and other markers of hepatocellular injury [28–30]. However, despite receiving accelerated approval by the FDA in 2016 as second-line treatment for PBC patients which don't respond to primary treatments, post-market safety monitoring identified several cases of drug-induced liver injury in those receiving higher doses of OCA [31,32]. Furthermore, while RCTs with metabolic dysfunction-associated fatty liver disease (MAFLD) and MASH patients demonstrated improved clinical outcomes with OCA, including reduced fibrosis, improved histological features of MASH and decreased biochemical markers of liver injury, inflammation and oxidative stress, these trials highlighted adverse events, including dose-dependent dyslipidaemia with worsening of the high-density lipoprotein/low-density lipoprotein ratio also in patients receiving higher doses (25 or 50 mg) of OCA [28,33–35]. A common adverse event in both PBC and MASH patients was the induction of significant pruritis, and while the underlying mechanisms are poorly understood, activation of pruritis by non-bile acid, structurally diverse FXR agonists suggests a receptor-mediated class effect [36,37].

Emerging clinical data have highlighted the complexity of FXR signalling and the far-reaching effects of its activation, emphasising the need for ligands to not only activate FXR specifically but also to modulate FXR actions selectively. While certainly challenging, this can be achieved by the manipulation of different receptor conformations, allosteric regulation of the ligand binding domain, and even remote communication between receptor domains [38]. FXR has shown considerable promiscuity and can be activated by diverse ligand chemotypes, including steroidal agonists such as bile acids and OCA, or non-steroidal agonists such as isoxale GW4064, Tropifexor and Fexaramine [39–43]. Furthermore, different ligand scaffolds and their associated receptor conformations have been shown to promote distinct target gene regulation, thought to be driven by different coactivator recruitment and usage [44,45].

In work presented here, we describe the search for a novel, more potent FXR agonist that could have the intended effect on key FXR-mediated metabolic pathways, while having limited systemic circulation to minimise undesirable off-target effects. A new generation of bile acid-derived compounds has been designed to include alternative functional groups along the cyclopentanophenanthrene steroid nucleus and replacement of the carboxylic acid moiety [46]. These modifications were anticipated to increase the specificity of the bile acid-based ligands for FXR, to drive alternative FXR conformations, and to alter the physicochemical properties and therefore, solubility and toxicity, of the prospective compounds [47]. We characterise the potency and efficacy of two novel bile acid-derived compounds on FXR activation, evaluating their ability to regulate bile acid homeostasis-related target genes *in vitro* and *in vivo*. Structural studies, performed in this work, identified that these compounds induce alternative binding mechanisms that may support selective coactivator recruitment and could offer more selective FXR activation.

Materials and Methods

Materials

All compounds (CDCA, OCA, compounds **1** and **2**) were provided by NZP UK Ltd (Reading, UK) for use in assays and work described herein, and are >95% pure as confirmed by HPLC analysis. Compounds 1 and 2 were synthesised and characterised by NMR spectroscopy, and purity confirmed by HPLC analysis, as described previously [46]. The SRC2-3 coactivator peptide (KENALLRYLLDKD) used for co-crystallisations was custom synthesised by Lifetein (New Jersey, USA). The GST-tagged FXR LBD was provided with the LanthaScreen™ TR-FRET FXR Coactivator Assay kit from Invitrogen (Massachusetts, USA). Additional terbium-labelled coregulator peptides were purchased also from Invitrogen. KiCqStart™ SYBR® Green Primers were purchased from Merck (UK). Huh7 cells were obtained from the Japanese Collection of Research Bioresources JCRB and HepG2 cells were a kind gift from Prof. Francesca Greco (University of Reading, UK).

Protein expression and purification

DNA encoding residues M257-Q472 of human FXR LBD (Q96RI1-2), with two surface mutations E277A and E350A, was synthesised and assembled directly in a pET15b vector with an N-terminal hexahistidine (His_6) tag by GenScript (Piscataway, NJ, USA). The plasmid was transformed by heat shock method into Rosetta (DE3) pLysS cells (Novagen). Starter cultures were grown from single colonies incubated overnight at 37 °C, shaking at 220 rpm, and in turn, used for inoculation into 8 L fresh LB medium. When cells had grown to mid-exponential phase, as determined by optical density at 600 nm (OD600), protein expression was induced by the addition of 0.5 mM (final concentration) isopropyl-β-D-thiogalactopyrano side (IPTG). Following induction, cells were incubated for a further 16 h at 16 °C and finally harvested by centrifugation (5000*g* for 15 min at 4 °C).

For purification of overexpressed FXR LBD, whole cell pellets were resuspended in lysis buffer (50 mM Tris–HCl pH7.8, 500 mM NaCl, 30 mM

imidazole, 0.2% (v/v) tween20, 10% (v/v) glycerol) supplemented with cOmplete™ EDTA-free protease inhibitor cocktail tablets, lysozyme (0.5 mg/mL) and DNase I (400 U/mL). Cells were lysed using a continuous flow cell disruptor at 30kPsi (Constant Systems, UK) and the crude lysate was clarified by centrifugation (30,000*g* for 45 min at 4 °C). The resulting supernatant was separated and loaded directly onto a HisTrap™ HP immobilised metal affinity column (Cytiva, UK) pre-equilibrated with wash buffer (50 mM Tris–HCl pH7.8, 500 mM NaCl, 30 mM imidazole). Unbound proteins were removed by washing and His_6-tagged proteins were eluted in a high imidazole concentration buffer (50 mM Tris–HCl pH7.8, 500 mM NaCl, 500 mM imidazole, 10% (v/v) glycerol). The His_6 tag was cleaved by the addition of thrombin (10U/mg protein) and dialysed overnight at 4 °C against 50 mM Tris–HCl pH8.3, 100 mM NaCl, 10% (v/v) glycerol, 0.1% CHAPS, 1 mM DTT. Cleaved protein was subjected to another purification on a HisTrap™ HP column and unbound protein was collected for further purification on a HiLoad Superdex™ 16/600 size exclusion column (Cytiva, UK) pre-equilibrated with gel filtration buffer (50 mM Tris–HCl pH7.9, 500 mM NaCl, 10% (v/v) glycerol, 1 mM DTT). Following gel filtration, fractions were verified by SDS-PAGE, and those containing FXR-LBD protein were pooled and buffer exchanged into 10 mM Tris–HCl pH8.3, 100 mM NaCl, 1 mM DTT.

Structure determination

A protein/ligand/coactivator complex was formed by incubation of the purified FXR LBD protein with a 12-times molar excess of either compound **1** or **2** (dissolved in 100% DMSO) and a five times molar excess of a SRC2-3 coactivator peptide (dissolved in water). After incubation overnight at 4 °C, the complex was concentrated using an Amicon Ultra® 15 (10,000 molecular weight cut-off) centrifugal philtre. Crystals formed at protein concentrations of 9.4 mg/ml in complex with compound **1**, and 32 mg/ml in complex with compound **2**, both with SRC2-3 coactivator peptide. Crystallisation screens were set up using an Oryx8 crystallisation robot dispensing 200 nL protein complex solution and 200nL precipitating solution in a sitting drop vapour diffusion setup. Crystals of protein complexed with compound **1** were formed with the Ligand Friendly Screen (Molecular Dimensions, UK) condition C10 (0.1 M HEPES pH7.0, 0.1 M $MgCl_2{\cdot}6H_2O$, 20% PEG6000, 10% ethylene glycol). Crystals were flash cooled in liquid nitrogen without cryoprotectant. Diffraction data were collected at the European Synchrotron Radiation Facility (France) beamline ID30A-1 (MASSIF-1). For protein complexed with compound **2**, diffraction-quality crystals were obtained from a solution of 0.1 M sodium phosphate dibasic, 0.2 M lithium sulphate pH 4.2, 20% PEG 2000 MME. Immediately prior to flash cooling in liquid nitrogen, crystals were cryoprotected by quick transfer through a mixture of reservoir solution and 20% ethylene glycol. Diffraction data were collected at Diamond Light Source (UK) beamline I03. Both datasets were solved by molecular replacement using FXR structure (pdb_00006HL1) as a template model and using the MOLREP programme implemented in CCP4 [48]. Structure refinement was carried out using PHENIX [49]. Refinement involved initial rounds of rigid body and simulated annealing, followed by real-space refinement. Manual model building, during the iterative refinement steps, was accomplished using COOT [50]. Polder OMIT maps were generated in PHENIX to verify the presence of ligand densities in the binding pocket and can be found in Supplementary Figure 1. Water molecules were added both manually and automatically (using PHENIX) to the structure solution. Validation of the final model was accomplished using MolProbity [51]. The data collection and refinement statistics, generated using PHENIX, are provided in Supplementary Table 1. Graphic representation and interpretation of the structures were performed using PYMOL (Version 1.7.4 Schrödinger, LLC.) and CCP4mg [52].

Coregulator recruitment

The recruitment of coregulator peptides to the FXR LBD was measured using a LanthaScreen™ TR-FRET FXR Coactivator Assay (Invitrogen). The assay was performed according to the manufacturer's instructions in 384-well plates using 20 μl reactions per well and using GST-tagged FXR LBD provided with the kit. Reaction mixtures contained components to the final concentrations of 5 nM Terbium anti-GST antibody, 10 nM GST-tagged FXR LBD, and varying serial concentrations of ligand compounds in DMSO (1% v/v) or varying serial concentrations of fluorescein-labelled coregulator peptide. Measurements were carried out on a FlexStation® 3 microplate reader using the LanthaScreen module (excitation at 340 nm, emission at 488 nm and 518 nm, 50 μs delay time, and 400 μs integration time). Individual reactions were replicated in 4 wells and 3 independent experiments were carried out. Raw data were normalised to DMSO-only controls (without ligand compound) and controls without FXR LBD-GST were performed for an indication of autofluorescence. Data are depicted as ratiometric measurements of donor and acceptor fluorescence. Data were plotted in GraphPad Prism (GraphPad Software Inc., San Diego, USA) using the four-parameter log-logistic model to fit the non-linear regression variable slope.

Cell culture

Huh7 cells were cultured in Dulbecco's Modified Eagle Medium supplemented with 10% FBS and 2 mM L-glutamine. HepG2 cells were grown in Eagle's Minimum Essential Medium supplemented with 10% FBS, 2 mM L-glutamine, and 1% non-essential amino acids. All cells were grown and maintained at 37 °C and 5% CO_2. Cells were seeded in 6-well plates (1×10^6 cells per well) in the same medium and left to adhere. Twenty-four hours after seeding, the medium was removed from each well and replaced with medium additionally containing OCA (300 nM or 1 μM) or the test compounds **1** (92 nM or 400 nM) and **2** (27 nM or 180 nM) in DMSO, or DMSO alone as control (final concentration 1% DMSO). Cells were incubated with test compounds for either 6 or 24 h before being harvested, washed with cold Dulbecco's PBS, and then directly used for RNA extraction. Each plate was replicated in 3 independent experiments.

Animals and compound administration

All procedures involving the animal husbandry, housing, and treatment of mice were carried out by Saretius Ltd (Reading, UK) under licence from the Home Office and in accordance with The Animals (Scientific Procedures) Act 1986. Mice (C57BL6J) were obtained from Charles River Laboratories (UK) and housed under standard conditions (temperature-controlled room and maintained in 12-h light/12-h dark cycles). Age and weight-matched groups (n = 10 per treatment group) of 10–12-week-old male mice were used. Mice were dosed with either DMSO (5% v/v, control), OCA (30 mg/kg body weight) or compound **1** (30 mg/kg body weight) in a vehicle of 0.5% methylcellulose in water. Mice were dosed by oral gavage (p.o) once a day (q.d.) for 5 days, and animals were given free access to food and water. On the 5th day, food was removed 30 min prior to the final treatment, and after compound administration, mice were starved for a further 6 h before being sacrificed. Mice were euthanised by schedule 1 CO_2 administration and livers harvested. Left lobe liver sections were lysed for total RNA extraction using a round-bottom glass homogenizer.

RNA extraction and RNA-sequencing

Two micrograms of total RNA were extracted from (above described) cells or mouse livers using the RNAqueous™ Total RNA Isolation kit (Ambion), according to the manufacturer's instructions. RNA concentration, integrity and quality was checked using a NanodropOne spectrophotometer and Qubit 4 Fluorometer. For mouse RNA, library preparation with PolyA selection was performed by Genewiz, AZENTA Life Sciences (Germany). Paired end 150-bp sequencing with a read depth of 20 million was performed using an Illumina Novaseq by Genewiz, AZENTA Life Sciences (Germany).

RNA-sequencing analysis

Sequence reads were trimmed using Trimmomatic v.0.36 and mapped to GRCm38 *Mus musculus* reference genome using the STAR aligner v.2.5.2b. Unique gene hit counts were identified using featureCounts from the Subread package v.1.5.2 and differential gene expression between the different treatment groups was performed using DESeq2 and the Wald test to identify genes with an adjusted p-value <0.05 and absolute log2 Fold change >1; these were determined to be differentially expressed genes. Significantly differentially expressed genes were analysed for functional enrichment by the over-representation of Gene Ontology terms using g:Profiler (version e113_eg59_p19_f6a03c19) with g:SCS multiple testing correction method applying significance threshold of 0.05 [53]. Volcano plots and Bubble plots were generated and edited using SRplot [54]. Gene lists of significantly upregulated and significantly downregulated genes were independently inputted into the Cytoscape software (version 3.10.2) [55] and the STRING app [56] used to visualise interactions between the protein products of these genes. Functional enrichment was performed on these independent gene lists also within the STRING app and filtered against the Wikipathways database [57]. Pathway terms were annotated directly on the network maps and images exported directly from Cytoscape.

Reverse transcription, and RT-qPCR analysis

Total RNA was DNase I treated before first strand cDNA synthesis. RNA was reverse transcribed into cDNA using the iScript Advanced cDNA Synthesis kit (BioRad). FXR target gene expression was analysed by RT-qPCR using a StepOnePlus™ system (Life Technologies) and iTaq Universal SYBR Green Supermix (BioRad). KiCqStart® SYBR® green primers were purchased from Sigma-Aldrich. Primers were added to each reaction to a final concentration of 500 nM and approximately 5 ng cDNA was added to each well. Each sample was set up in triplicate. Target gene Ct values were normalised to GAPDH for Huh7 and HepG2 derived samples and Cox7a2L for mouse liver-derived cDNA. Treated samples were displayed relative to untreated controls (DMSO only) using the ΔΔCt method [58].

Statistical analysis

Gene expression data from RT-qPCR experiments were displayed as mean ± SEM. Statistical analysis was performed on normalised

ΔCt values using SPSS software (IBM, NY, USA). Data were first analysed by Shapiro-Wilk and Levene's tests, followed by One-way ANOVA with Tukey's or Bonferroni's post hoc test. Statistical significance was shown as $*p < 0.05$, $**p < 0.01$, $***p < 0.001$.

Results

In a search for novel FXR agonists, a chemical compound library (proprietary to NZP UK Ltd, Reading, UK), comprising bile acid-derived molecules, was screened in a cell-based FXR reporter assay (performed by Indigo Biosciences Inc., State College, PA, USA). Compounds were tested in a cell-based TGR5/cAMP assay (Eurofins Cerep, Celle L'Evescault, France) and screened against a panel of 78 human cell-surface receptors for pharmacological profiling (SAFETYscan® by Eurofins DiscoveRx, Fremont, CA, USA). The screens identified compounds **1** and **2** (Figure 1C), which had a high affinity for FXR, without activation of TGR5 or cross-reactivity with other off-target receptors at concentrations below 100 μM [46] (Supplementary Figure 2).

Novel compounds adopt unique binding modes occupying the entire ligand binding pocket of FXR

To rationalise the agonism of compounds **1** and **2**, and to identify the molecular basis for their activation of FXR, X-ray crystallographic structures of FXR LBD complexed with either compound **1** or compound **2** were determined. Co-crystals of FXR LBD with compound **1** and the coactivator peptide, SRC2-3 diffracted to a resolution of 3.1 Å (pdb_00009H65). The structure corresponds to space group I222, giving 2 identical monomers in the asymmetric unit. The crystallographic statistics are presented in Supplementary Table 1 and the final structure is shown in Figure 2A. Both monomers adopt the 12-α-helical sandwich arrangement typical of FXR LBD structures, and both were complexed with one molecule of **1** and one steroid receptor coactivator (SRC) 2–3 peptide. Ligand binding interactions were analysed, and the determined structure was superimposed with the structure of FXR LBD in complex with OCA (pdb_00001OSV) for comparison. Superimposition of the two structures demonstrated a root mean square deviation (RMSD) of 0.606 Å for chain A (204 alpha-carbon atoms), and 0.664 Å for chain B (199 alpha-carbon atoms). While the cyclopentanophenanthrene backbones of the two structurally analogous compounds aligned almost identically in the same canonical binding site, the structure of FXR LBD with **1** displayed notable shifts in the helices and the flexible loop regions near the pocket entrance, which were likely displaced to accommodate the additional steric bulk in the extended side chain of compound **1** (Figure 2B). Similarly to OCA, **1** mimics the classic bile acid binding orientation, with its 'A'-ring 'headfirst' in the cavity closest to helix 7 and helix 11. In this position, the C3 hydroxyl group on the 'A'-ring is ideally located for polar interactions with the established activation trigger residues Tyr361 (helix 7), and His447 (helix 11) which in turn engages the perpendicular Trp469 (helix 12) in a cation-π interaction that constrains helix 12 in an active conformation, as observed previously [5]. As with other traditional bile acids, compound **1** is further stabilised in the pocket by additional hydrogen bonds between the C7 hydroxyl group and Ser332 (helix 5) and Tyr369 (helix 7), supported by several complementary non-polar and hydrophobic interactions surrounding the steroidal backbone (Figure 2C). While substitution of the bile acid's typical carboxylic moiety with the benzene sulfonylurea of **1** is sufficient to maintain polar interactions with Arg331 at the pocket entrance, the extended side chain is positioned adjacent to helix 3, and functional groups are well placed for additional hydrogen bonds with Thr270 on the loop between helix 1 and 2 (Figure 2B).

Co-crystals of FXR LBD complexed with compound **2** and SRC2-3 diffracted to a resolution of 2.6 Å (pdb_00009H66). In this instance, the structure contained 4 monomers in the asymmetric unit and corresponded to space group $P2_1$ (Supplementary Table 1). All four monomers were bound with one molecule of **2** and at least one molecule of coactivator peptide (Figure 3A). As with **1**, compound **2** was found to adopt the standard bile acid orientation in the primary ligand pocket, where it could make polar interactions with core residues His447, Tyr361, Tyr369, and Ser332 (Figure 3B, C). Superimposition of FXR complexed with OCA (pdb_00001OSV) demonstrated RMSD values of 0.491 Å, 0.643 Å, 0.634 Å, 0.590 Å (for 197–208 alpha-carbon atoms) for chains A, B, C and D respectively. Both structures demonstrated an overlapping steroid nucleus of **2** and OCA in the main bile acid cavity (Figure 3B). Likewise, while stabilisation of the receptor can be facilitated by several polar, electrostatic, van der Waals, and hydrophobic interactions with atoms across the cyclopentanophenanthrene backbone, the extended side chain of **2** affords novel interactions not seen in the OCA binding mechanism (Figure 3B, C). Likewise, the subtle structural differences between compound **1** and **2**, such as the additional amide linkage of compound **1**, and the additional trifluoromethoxy group of compound **2**, confer varying degrees of flexibility around these functional groups, driving distinct interactions with the receptor, sufficiently producing small shifts in FXR conformation. Along

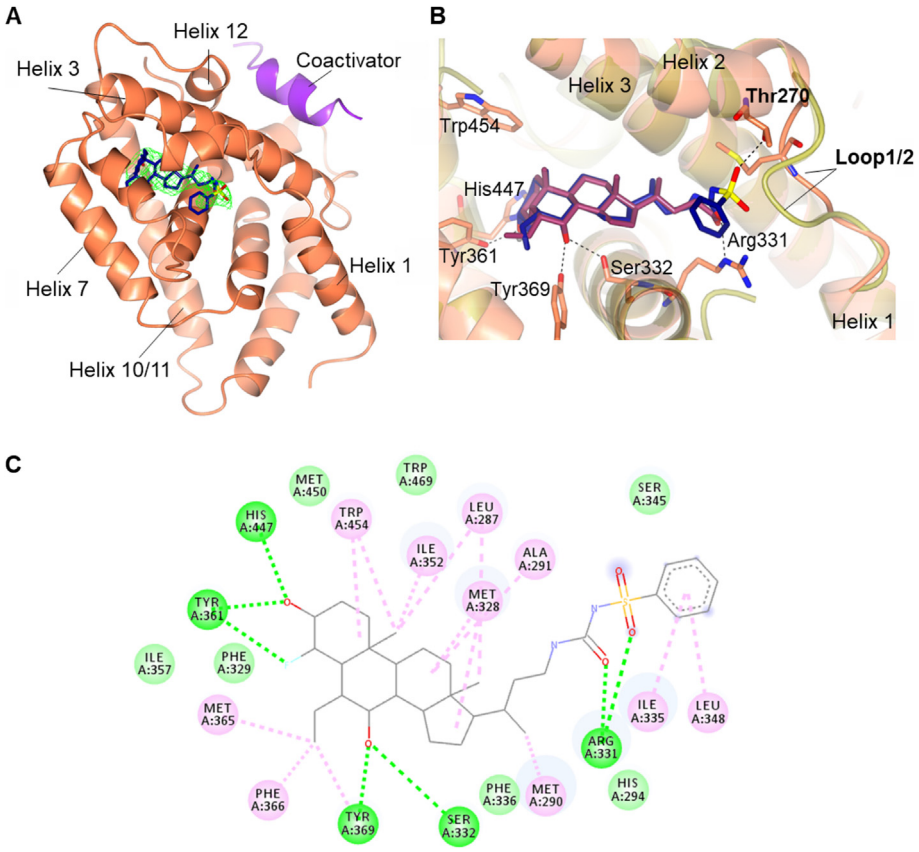

Figure 2. Structure solutions of the FXR LBD bound with compound 1. (A) Ribbon structures of FXR LBD (coral) complexed with **1** (navy) and SRC2-3 peptide (purple). (**B**) Superimposition of FXR LBD-compound **1** (coral/navy) and FXR LBD-OCA (gold/violet, pdb_00001OSV) show the alignment of the steroid backbone of both compounds, with side chain differences. Residues involved in ligand binding are indicated in bold. Polar interactions are indicated by a dashed line. Helix 1, 2 and 3 and the loop region between helix 1 and 2 at the pocket entrance are indicated. (**C**) Ligand interaction map between compound 1 and the FXR LBD. Interactions as displayed in Biovia Discovery Studio Visualizer v.19 (Dassault Systemes, San Diego, USA). Conventional hydrogen bonds (lime green), van der Waals (pale green), alkyl/pi-alkyl interactions (pink).

with anchoring Arg331 at the pocket entrance, the additional benzene sulfonyl pentanamide group of compound **2** occupies a supplementary pocket created between helix 3 and the helix 1–helix 2 loop (loop 1/2), which also has been described as an alternative 'back door' binding site [59]. Here, the side chain can engage Asn293 (helix 3) in a hydrogen bond (Figure 3B, C). Furthermore, the trifluoromethyl group at the distal end of the compound's side chain is responsible for fluorine-mediated contacts with Tyr260 (loop1/2), and Val297 (helix 3) (Figure 3D).

In addition to indirectly contributing toward the stabilisation of helix 12, helix 3 forms part of the coactivator recruitment site [60,61]. The structure of FXR LBD in complex with compound **2** determined here shows, that while two of the four monomers were complexed with a single SRC2-3 peptide bound in the primary groove described in other FXR LBD structures, two of the chains contained an ancillary SRC2-3 peptide in an adjacent groove (Figure 3E). It is possible that the second peptide is a crystallisation packing artefact due to its location at the interface between two monomers within the asymmetric unit. However, one of the monomers in the OCA-bound FXR structure (pdb_00001OSV, chain B) is also incidentally co-crystallised with a secondary coactivator peptide and superimposition of these novel complexes onto this monomer resulted in RMSD values of 0.488 Å for chain A (for 211 alpha-carbon atoms) and 0.479 Å for chain C (for 208 alpha-carbon atoms). As previously posited, it is plausible that additional coactivator association is due to ligand-induced structural changes [5]. In its typical binding site, the SRC2-3 peptide is oriented perpendicularly to helix 12, with its N- terminus towards helix 12 and C- terminus positioned towards helix 3 and 4. The hydrophobic leucine residues of the LXXLL interaction motif are buried in the groove created by helix 12 displacement, and polar interactions between the peptide and Glu314 and Glu467 on helix 3 and

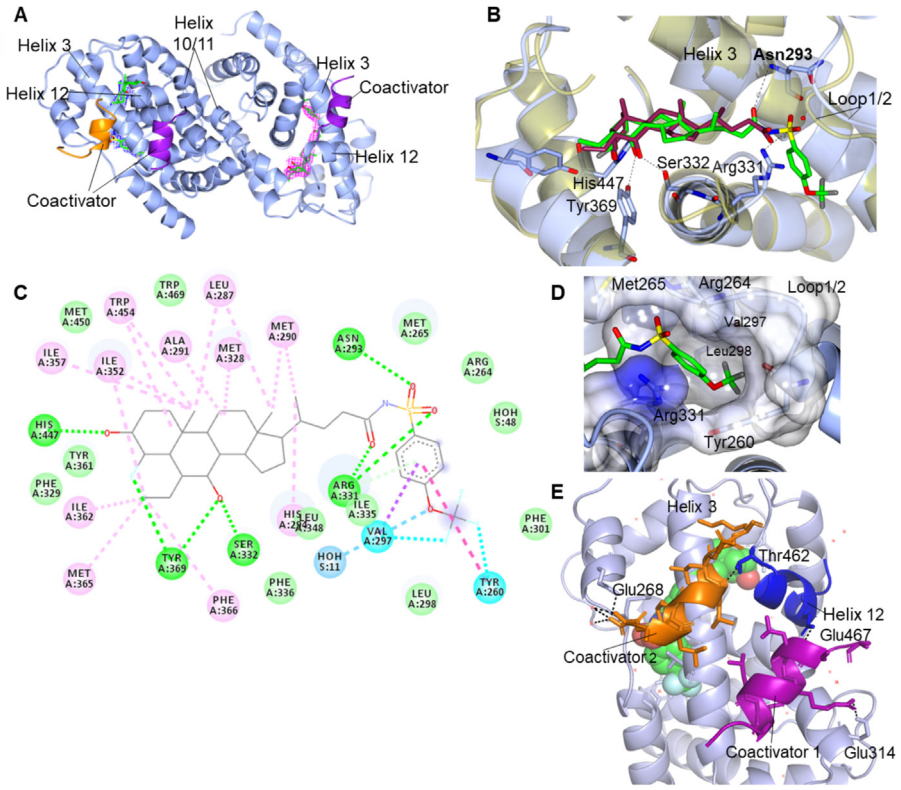

Figure 3. Structure solutions of the FXR LBD bound with compound 1. **(A)** Ribbon structures in the asymmetric unit of two identical FXR LBD molecules (ice blue) complexed with **2** (lime) and primary SRC2-3 peptide (purple) and secondary SRC2-3 peptide (orange). (**B**) Superimposition of FXR LBD-compound **2** (ice blue/lime) and FXR LBD-OCA (gold/violet, pdb_00001OSV) shows the alignment of the steroid backbone of both compounds, with side chain differences. (**C**) Ligand interaction map of compound 2 and interacting residues of the FXR LBD. Conventional hydrogen bonds (lime green), van der Waals (pale green), alkyl/pi-alkyl interactions (pink), pi-sigma (purple), halogen/fluorine (cyan). (**D**) Occupancy of the alternative sub pocket with compound **2**'s extended side chain. Surface showing the cavity created by residues between helix 1, 2, 3, and 5. (**E**) Structure of chain A showing primary (purple) and secondary (orange) coactivator peptides in the adjacent binding grooves between helix 3 and 12. Residues involved in ligand binding are indicated in bold and shown as sticks. Polar interactions are indicated by a dashed line.

12, respectively, further stabilise its association (Figure 3E). Although binding in an anti-parallel fashion compared to the primary coactivator peptide, the secondary peptide also supports a disposition where its hydrophobic leucine residues are buried into the surface between helix 3 and 12. Similarly, clamp-like polar interactions between the peptide and Glu268 (helix 2) and Thr462 (helix 12) can secure the recruited coactivator. It's possible that filling of the alternative sub-pocket with the extended side chain and subsequent interactions with residues on loop 1/2, helix 2, and helix 3, alters helix 3 packing against the peripheral coactivator binding site and expands the available surface area utilised for coactivator recruitment.

With both the canonical, steroidal binding site and the secondary, modulatory site being occupied by our novel ligands, we sought to identify whether the novel binding conformations of compounds **1** and **2**, consequentially, exhibited any unique activity regarding transcriptional cofactor recruitment, and ultimately what their respective effects would be on FXR target gene regulation.

Novel compounds exhibit higher potencies than CDCA or OCA in promoting coactivator peptide recruitment

To further characterise **1** and **2** as agonists for FXR and to investigate their ability to promote coactivator association with the FXR LBD, a time-resolved fluorescence resonance energy transfer (TR-FRET)-based coactivator recruitment assay was used. Initial assays were performed by recruiting a peptide, derived from the steroid receptor coactivator 2-2 (SRC2-2) motif, using increasing concentrations of compounds. This determined the half maximal effective concentration (EC_{50}) and potency of both novel compounds (Supplementary Figure 3). Steroidal agonists CDCA and OCA were used as control

ligands. Assays demonstrated that both **1** and **2** had a higher potency of SRC2-2 recruitment compared with either CDCA or OCA, with at least 4-fold lower EC_{50} values than OCA (Supplementary Table 3). However, while **2** was the most potent, **1** achieved the highest efficacy in all assays recruiting SRC2-2.

The assay was then repeated, using a panel of 8 different coregulator peptides, each containing nuclear receptor interaction motifs derived from naturally occurring coactivator and corepressor proteins, or peptides with coregulator-like motifs identified by random phage display (Invitrogen). Again, the assays were performed using increasing concentrations of CDCA, OCA, and compound **1** or **2** (dose–response curves shown in Supplementary Figure 4). Results showed that certain coactivator peptides (e.g. SRC2-2) exhibited substantial recruitment to the agonist-bound FXR LBD, whereas others (e.g. SRC1-1, SRC3-1) were not recruited at all, despite the supersaturating concentration of agonist used (Figure 4A). Assays using the corepressor peptide NCoR-1 did not display any increases in TR-FRET emission ratio, compared to the DMSO control, confirming that the compounds could not induce associations between the LBD and corepressor, and were indeed agonists. Despite recruiting different coactivator peptides to varying levels, compound **1** exhibited consistent potency in facilitating coactivator interaction with the FXR LBD, with EC_{50} values between 11 and 12 nM (Supplementary Table 4). The potency of compound **2** was more varied with EC_{50} values ranging between 9 and 35 nM dependent on the coactivator being recruited. Compound **2** had the highest potency when recruiting the SRC2-3, the same motif used in crystallisation studies, to the complex.

Compound **1** was tested in assays recruiting a further 16 coactivator peptides, where again it was found to produce a narrow range in EC_{50} values between 9 and 17 nM, but relatively substantial differences in the maximum TR-FRET ratio dependent on the coactivator peptide being recruited (Supplementary Table 5, Figure 4B). Peptides of SRC2-2, TRAP220/DRIP-1, and RIP140 L8 motifs displayed some of the biggest increases in TR-FRET signal upon ligand binding and, as representatives of three different coactivator families all derived from naturally occurring proteins, these were selected for further assessment. Although coactivator peptide SRC2-3 did not induce very large changes in TR-FRET, it

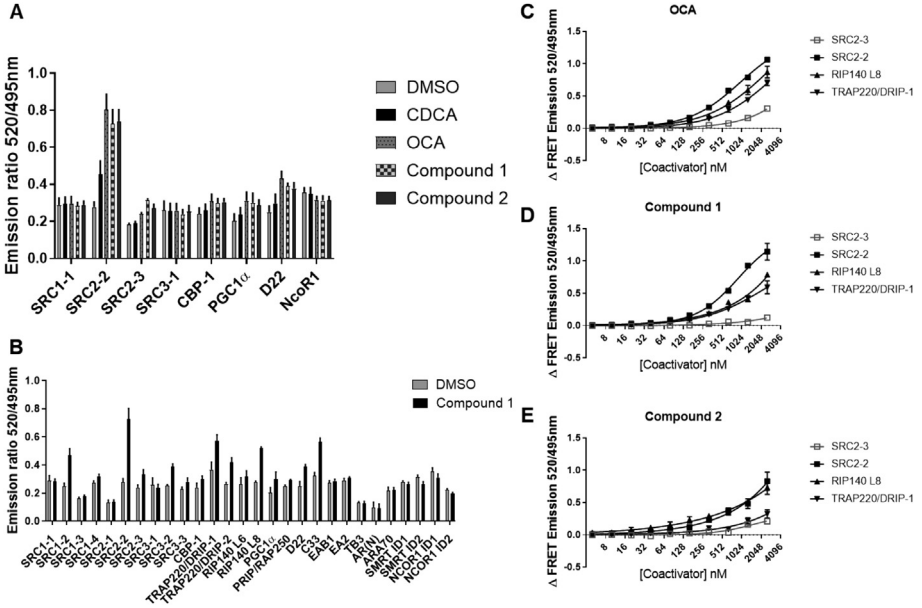

Figure 4. Coregulator peptide recruitment to ligand-bound FXR LBD as measured by TR-FRET ratio. (**A**) Maximal TR-FRET ratios observed with either CDCA, OCA, compounds **1,** or **2** were determined by the recruitment of different fluorescein-labelled coregulator peptides to the FXR LBD which was indirectly labelled (by a GST-tag and terbium-labelled anti-GST antibody). TR-FRET ratios displayed here represent assays using agonist concentrations of 10 μM (**B**) Maximal TR-FRET ratios were observed with a total of 28 different coregulator peptides when compound **1** (10 μM) occupied the FXR LBD compared to DMSO solvent control (for ligand-independent binding). Data are shown as mean ± SEM, (n = 3 independent experiments). (**C**–**E**) Peptides corresponding to the SRC2-2, SRC2-3, RIP140 L8, or TRAP220/DRIP-1 motifs on the respective coactivator proteins were serially diluted into reactions containing the GST-tagged FXR LBD saturated with 10 μM agonist (OCA (**C**), compound **1** (**D**) or compound **2** (**E**)). Changes in FRET emission ratios are displayed minus emission ratios from control assays without FXR LBD (to account for diffusion-enhanced FRET). Data are shown as mean ± SEM, (n = 3 independent experiments).

was included in further assessments to provide additional clarity around the crystallography results.

FXR has a distinct ligand-dependent co-regulator binding effects

To evaluate the propensity of the FXR LBD to recruit the selected coactivators, and to determine whether differences in recruitment are dependent on the ligand occupying the binding pocket, assays were performed by titrating the coactivator peptides while saturating the FXR LBD with the agonist. The concentrations of coactivator peptides used weren't sufficient to achieve full saturation of the receptor, however, the compounds appeared to induce notable differences in coactivator recruitment profiles (Figure 4C–E). When 10 μM OCA occupied the FXR LBD, SCR2-2, RIP140 L8, and TRAP220/DRIP-1 peptides appeared to be recruited equally, whereas the SRC2-3 coactivator was recruited to a lesser extent. Conversely, compound **1**-bound FXR LBD appeared to display stronger recruitment of SRC2-2 than the other coactivator peptides, and again SRC2-3 displayed the least changes in TR-FRET signal. Compound **2**, on the other hand, showed no clear preference for SRC2-2, but favoured equally SRC2-2 and RIP140 L8, over TRAP220/DRIP-1 and SRC2-3. Despite being recruited to the FXR LBD the least compared with other coactivator peptides tested here, SRC2-3 displayed higher changes in TR-FRET when the FXR LBD was complexed with OCA and compound **2**. This preferential coactivator recruitment may explain why FXR LBD bound with both OCA and compound 2 were co-crystallised with multiple peptides of SRC2-3 coactivator, whereas the compound 1-bound FXR LBD structure only contained one coactivator molecule. Recruitment profiles shown here, suggest a distinct association with these coactivator peptides, according to the ligand bound to the receptor. Whether this preferential recruitment of transcriptional coactivators results in distinctive changes to FXR target gene regulation was next investigated.

Novel compounds are more effective at regulating FXR target genes than OCA in vitro

Compounds **1** and **2**, alongside OCA as a reference compound, were evaluated for their *in vitro* effects on downstream FXR signalling. Human hepatoma HepG2 and Huh7 cells were treated with OCA, compound **1**, or compound **2** for 6 or 24 h. Compounds were used at their respective EC_{50} or EC_{90} concentrations (as determined by initial cell-based FXR-reporter assays conducted by Indigo Biosciences Inc). Messenger RNAs of FXR target genes were assayed by real-time quantitative PCR (RT-qPCR) and normalised to the reference gene GAPDH. Results showed that both **1** and **2** could regulate FXR target genes involved in bile acid homeostasis in a dose-dependent manner (Figure 5A). Gene induction of SHP and FGF19 was evident after 6 h of treatment with both compounds, but statistically significant decreases in CYP7A1 and increases in OSTα were more pronounced after 24 h of treatment with **1** and **2**. At their respective effective test concentrations, **1** appeared to be equally as efficacious as OCA, whereas **2** was more efficient than OCA at upregulating SHP, FGF19, and OSTα, while downregulating CYP7A1 mRNA.

Compound 1 displays an excellent ADMET profile for progression as a lead candidate

Compounds **1** and **2** were evaluated for their ADMET properties in various assays where it was noted that compound **2** had less favourable drug-like properties that would hinder its progression as a pharmacological drug candidate. When tested in Huh7 cells for viability, **1** did not display any toxicity, but **2** was not as well tolerated at 10 μM concentrations, as determined by fluorescence-based live cell multiplex assays (Supplementary Figure 6). Initial assays also indicated that compound **2** had a distribution coefficient (LogD) value of 5.7, indicating potential problems with absorption and restricted distribution of the compound, whereas **1** had much more favourable lipophilicity properties for cell activity and oral bioavailability. Both compounds were tested in Caco-2 cell permeability assays where compound **1** demonstrated a moderate permeability with a P_{app} (A > B) value of 6.10×10^{6} cm/s. Compound **2** however, was not detected in the receiver compartment when assays were run in the apical to basolateral direction (A > B), again suggesting potential solubility issues and poor absorption (Supplementary Table 6). Both compounds displayed permeability in the basolateral to apical direction (B > A) and compound **1** demonstrated a high efflux ratio of 2.25, suggesting possible active transport out of cells by multidrug resistance 1 (MDR1) or other transporters. To clarify further the absorption profiles of these compounds, both were tested for pharmacokinetic properties in C57BL6J mice. Following a single 50 μg dose administered orally of either compound, although similar half-lives ($t_{1/2}$) of both compounds, the peak serum concentration (C_{max}) of compound **1** was 3 times higher than that of compound **2,** suggesting absorption to a higher extent of **1**, and inadequate absorption of compound **2**. Furthermore, **1** had a 4-fold higher systemic exposure than compound **2**, with an area under curve (AUC_{last}) value of 1.774 h * μg/mL compared to 0.377 h * μg/mL, again indicating a more preferable bioavailability of compound **1** (Supplementary Table 7). Quantification of the compounds in mouse liver samples, identified

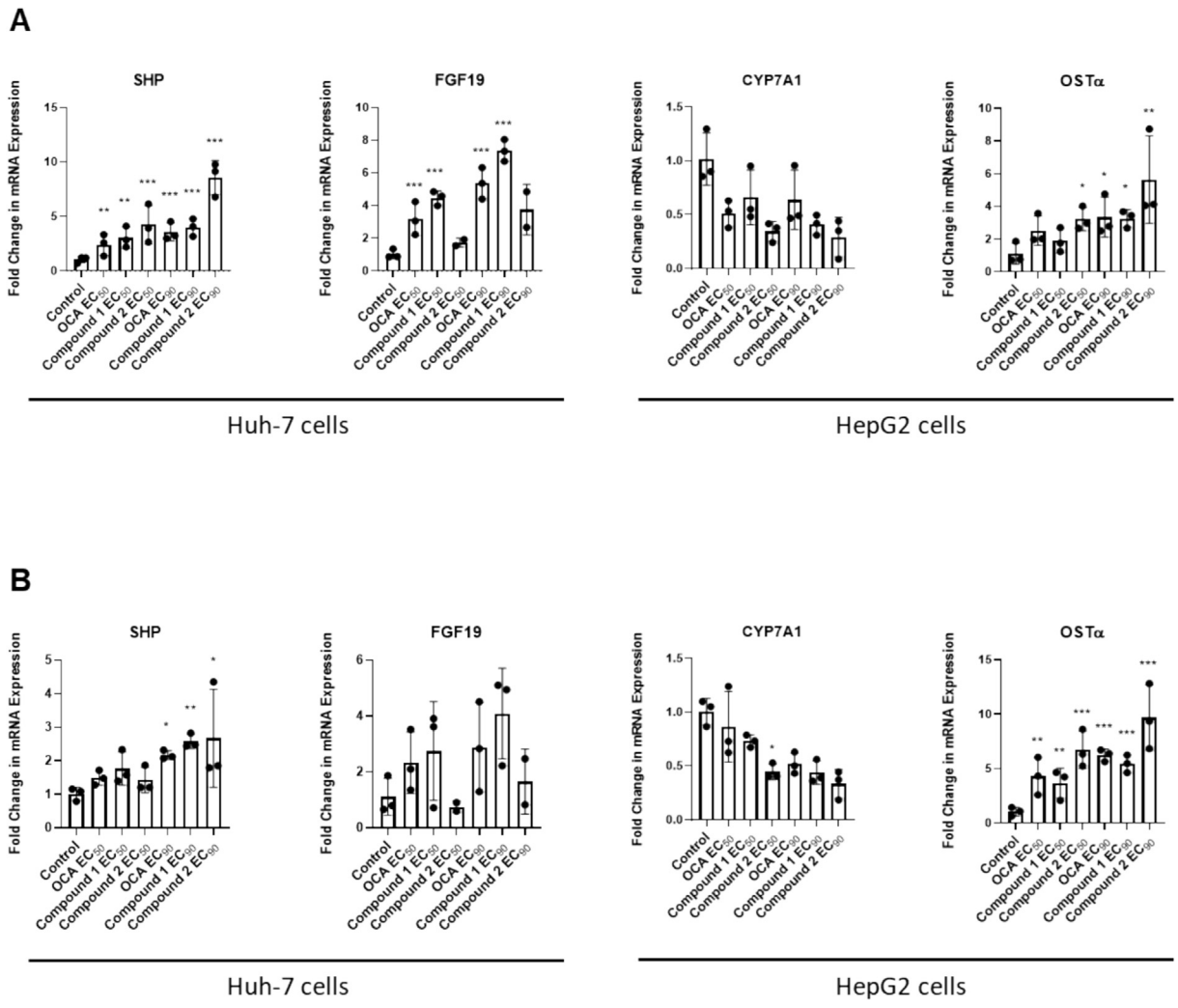

Figure 5. Novel compounds 1 and 2 regulate FXR target genes involved in bile acid homeostasis at (A) 6 h and (B) 24 h. The *in vitro* effects of compound **1** (EC_{50}: 90 nM; EC_{90}: 400 nM) and compound **2** (EC_{50}: 27 nM; EC_{90}: 180 nM) compared to OCA (EC_{50}: 300 nM; EC_{90}: 1000 nM) on mRNA expression levels of SHP, FGF19, CYP7A1 and OSTα relative to cells treated with DMSO (vehicle control). SHP and FGF19 expression were analysed in Huh7 cells, CYP7A1 and OSTα expression were analysed in HepG2 cells. Error bars represent ± SEM; Statistical analyses were performed using one-way ANOVA followed by Bonferroni's post hoc test. In cases where data were not normally distributed, a non-parametric Kruskal-Wallis test with Dunn's test was used. $^{*}p < 0.05$, $^{**}p < 0.01$, $^{***}p < 0.001$ versus vehicle control ($n = 3$ independent experiments).

higher liver exposure of compound **1** compared to **2** (Supplementary Figure 7). This verified the expected activity of compound **1** at the primary target site. However, the rapid decline in analyte concentration of compound **2**, suggests that the small amount absorbed and entering enterohepatic circulation is quickly metabolised or excreted from the liver, thereby limiting potential efficacy of **2** in the liver. Additional *in vitro* metabolic stability assays performed using both human and mouse liver microsomes, demonstrated that compound **1** was stable, with moderate to low intrinsic clearance (CLint) in humans and mice, respectively (Supplementary Table 8). Accordingly, with the data suggesting that compound **1** is not toxic to cells, sufficiently absorbed, moderately distributed to liver tissue, metabolically stable and may have good oral bioavailability, it was progressed as the lead compound in further studies.

Compound 1 and OCA favourably regulate different FXR target genes in vivo

To further investigate **1** and its global effects on gene regulation *in vivo*, male C57BL/6 mice were treated with either OCA or compound **1** for 5 days, and liver sections used for RNA-sequencing (RNA-seq). Due to interspecies bile acid metabolism differences, which account for higher

doses of steroidal compounds needed to elicit a response in rodent FXR, and in line with previous preclinical studies [26,29,62], mice were dosed with 30 mg/kg/day for both compounds. Compounds were administered daily in 0.5% methylcellulose vehicle by oral gavage (*p.o*) and compared with mice treated with vehicle only.

Differential gene expression analysis using a standard DESeq2 workflow, showed that treatment with OCA significantly induced differential expression in 268 genes (77 genes were upregulated and 191 genes were downregulated), whereas compound **1** treatment resulted in significant differential expression of 1368 genes (861 upregulated and 507 downregulated genes) (Figure 6B and C). Of the genes differentially expressed due to treatment with **1**, several were involved in pathways directly regulated by FXR or relevant to bile acid homeostasis and metabolism, including SHP, BSEP, OSTβ, Ileal Bile Acid Binding Protein (I-BABP) and Multidrug Resistance Protein 3 (MDR3), which were all upregulated; and CYP7A1, Sterol 12-Alpha-Hydroxylase (CYP8B1), Hepatocyte Nuclear Factor 1-Alpha (HNF1A) and Organic Anion Transporting Polypeptide 1 (OATP1), which were down-regulated. Of these bile acid-related genes only CYP8B1 was significantly regulated by OCA treatment, and there were no statistically significant differences in the expression of other classic FXR target genes. Validation of these results by RT-qPCR showed that hepatic expression of FXR targets SHP and BSEP was increased upon treatment with either compound (Supplementary Figure 9). Mice treated with 30 mg/kg OCA displayed 7-fold increases in SHP mRNA compared to 3.5-fold changes with compound **1** treatment, whereas increases in BSEP expression were slightly more pronounced with compound **1** treatment than with OCA. However, similarly to RNA-seq results, OCA treatment did not appear to significantly affect CYP7A1, while compound **1** treatment downregulated CYP7A1 mRNA 1.5-fold.

Compound 1 and OCA differentially regulate diverse gene pathways in vivo

RNA-seq results demonstrated that both compounds could induce differential expression in genes involved in multiple, diverse pathways aside from those related to bile acid metabolism and homeostasis. Functional profiling on the significant differentially expressed genes was performed and significantly over-represented gene ontology terms were identified using g:Profiler (version e113_eg59_p19_f6a03c19) [53]. The highlighting function within g:Profiler, a filtering algorithm which reorganises related GO terms and removes redundant terms, was used to identify the key driver terms shown in Figure 6(E–G). Due to the downregulation of several large and small ribosomal subunits genes, pathways that were significantly enriched with OCA-treatment included cytoplasmic translation (GO:0002181) and ribosomal small subunit biogenesis (GO:0042274) (Figure 6E). Other gene ontology biological processes associated with OCA ranged from oxidative phosphorylation and mitochondrial respiratory chain complex assembly, to negative regulation of carbohydrate metabolic process and acute-phase response (GO:0006119, GO:0033108, GO:0045912 and GO:0006953 respectively). Analysis of gene ontology terms of transcripts regulated by compound **1** showed significant enrichment in positive regulation of biological processes and cell cycle pathways (GO:0048518, GO:0007049) (Figure 6F). Compound **1** also enriched several biological processes involving metabolism including the lipid metabolic process, organic acid metabolic process, intracellular glucose homeostasis and regulation of gluconeogenesis and DNA metabolic process (GO:0006629, GO:0006082, GO:0001678, GO:0006111 and GO:0006259 respectively). In addition, compound **1** was responsible for the differential regulation of genes involved in regulatory processes such as regulation of transcription by RNA polymerase II and circadian regulation of gene expression (GO:0006357, GO:0032922). Sequencing results showed an overlap of 87 genes that could be regulated by both OCA and compound **1**, however, this represented only 5.6% of the total differentially expressed genes associated with both compound treatments (Figure 6A).

The Wald test was used to compare gene expression between OCA- and compound **1**-treated samples. Results showed a total of 670 significantly differentially expressed genes; 418 genes being upregulated, and 252 genes being downregulated in mice treated with compound **1** compared to mice treated with OCA (Figure 6D). Collectively, these genes were associated with different metabolic processes including small molecule metabolic process (GO:0044281), regulation of lipid metabolic process (GO:0019216), glutathione metabolic process (GO:0006749) and glucose homeostasis (GO:0042593). Differentially expressed genes between compound **1** and OCA treatment were further analysed by identifying networks and interactions between the protein products of the up- and downregulated genes. These networks were also profiled against the Wikipathways database to identify enriched functional pathways associated with the genes. Genes that were upregulated with compound **1** treatment compared to OCA treatment, indicated significant enrichment of pathways pertaining to cell cycle, circadian rhythm genes, glutathione metabolism and oxidative phosphorylation (WP179, WP3594, WP100, WP623 respectively) (Figure 7A), whereas downregulated pathways included FXR pathway and cholesterol biosynthesis,

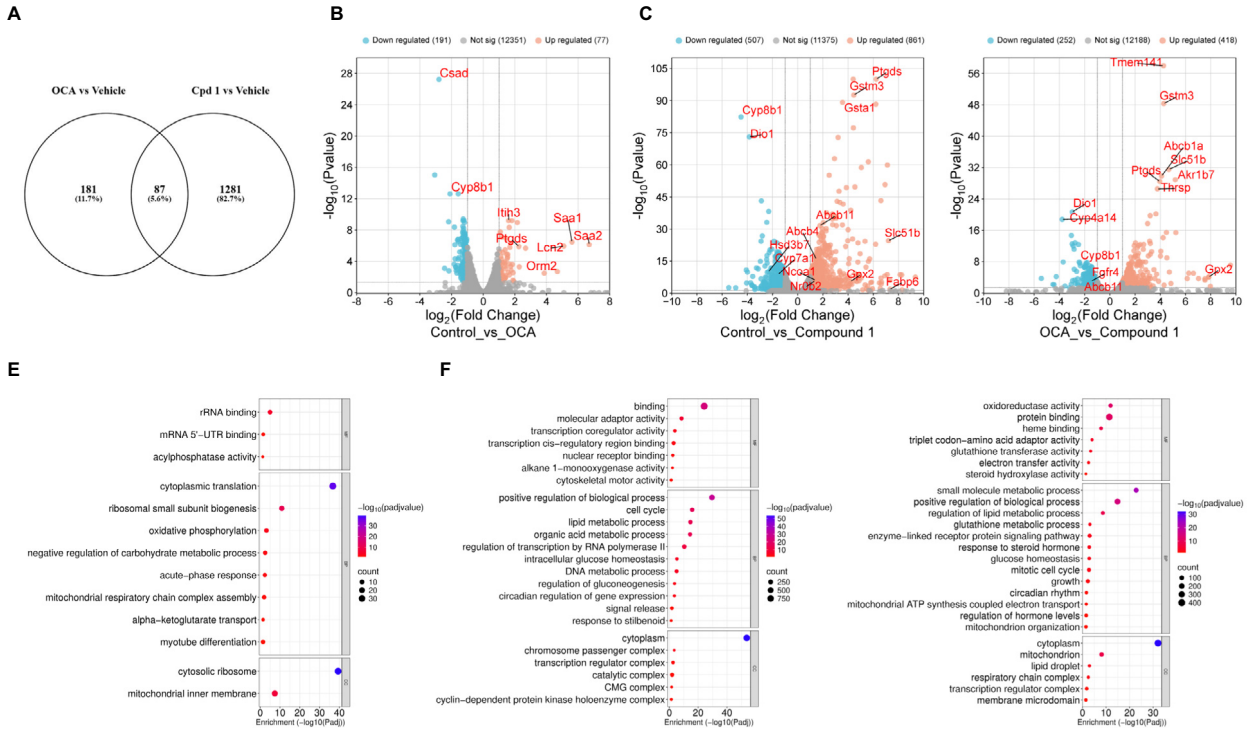

Figure 6. OCA and compound 1 differentially regulate gene expression. RNA-seq analysis of C57BL/6J mice treated once daily for 5 days with OCA or compound **1** (both at 30 mg/kg/day). Data are displayed relative to transcript levels of target genes in cells treated with vehicle (DMSO). (**A**) A Venn diagram showing the total number of differentially expressed genes induced by OCA, compound **1** and both treatments compared to vehicle treated mice. (**B**–**D**) Volcano plots of all genes significantly regulated by OCA compared to control (**B**), compound **1** both compared to control (**C**), and OCA compared to compound **1** (**D**). Red dots represent significantly upregulated genes, blue dots represent significantly downregulated genes. Volcano plots were generated for visualisation using SRplot [54]. (**E**–**G**) Gene Ontology analysis of enriched or depleted pathways associated with OCA treatment compared to control (**E**), compound **1** treatment compared to control (**F**) and compound **1** compared to OCA treatment (**G**). Colour is representative of negative $\log_{10}$ of adjusted *p*-value and disk size is proportional to the gene count. Gene ontology pathways are separated into Molecular Function (MF), Biological Process (BP) and Cellular Compartment (CC). Gene ontology analysis was performed using g:profiler [53] and Bubble plots were generated for visualisation using SRplot [54].

adipogenesis and glycolysis and gluconeogenesis pathways (WP2879, WP5329, WP236 and WP534 respectively) (Figure 7B). Overall, comparison between the two treatments revealed several unique gene ontology terms and Wikipathway annotations, further supporting the idea of distinct mechanisms of action of OCA and compound **1**.

Discussion

The underlying homeostatic role of FXR in several metabolic pathways has emphasised this receptor as an attractive therapeutic target. However, due to FXR's complex signalling network and widespread expression in various tissues and organs, receptor activation also results in mechanism-based side effects. Strategies to manipulate FXR's effects in a tissue- or function-specific manner are of considerable interest; whether by developing a highly potent agonist to limit administered doses and, as such, the systemic concentration of the compound, or by developing compounds that can selectively modulate the receptor.

Previous studies by Pellicciari et al. identified that modifications to the bile acid side chain could achieve modulatory effects on FXR activation [59]. Furthermore, the addition of fluorinated functional groups to compounds has been shown to alter the hydrogen bonding capacity of hydroxyl groups, and thus ligand-receptor interactions [63]. In this study, we present two novel steroidal agonists of FXR. These were identified by reporter gene screening of a small library of bile acid-derived compounds with additional fluorine-containing functional groups along the steroid nucleus and diverse substitutions of the carboxylic acid side chain. Initial screening of the library, identified that fluorinated compounds had higher affinities for

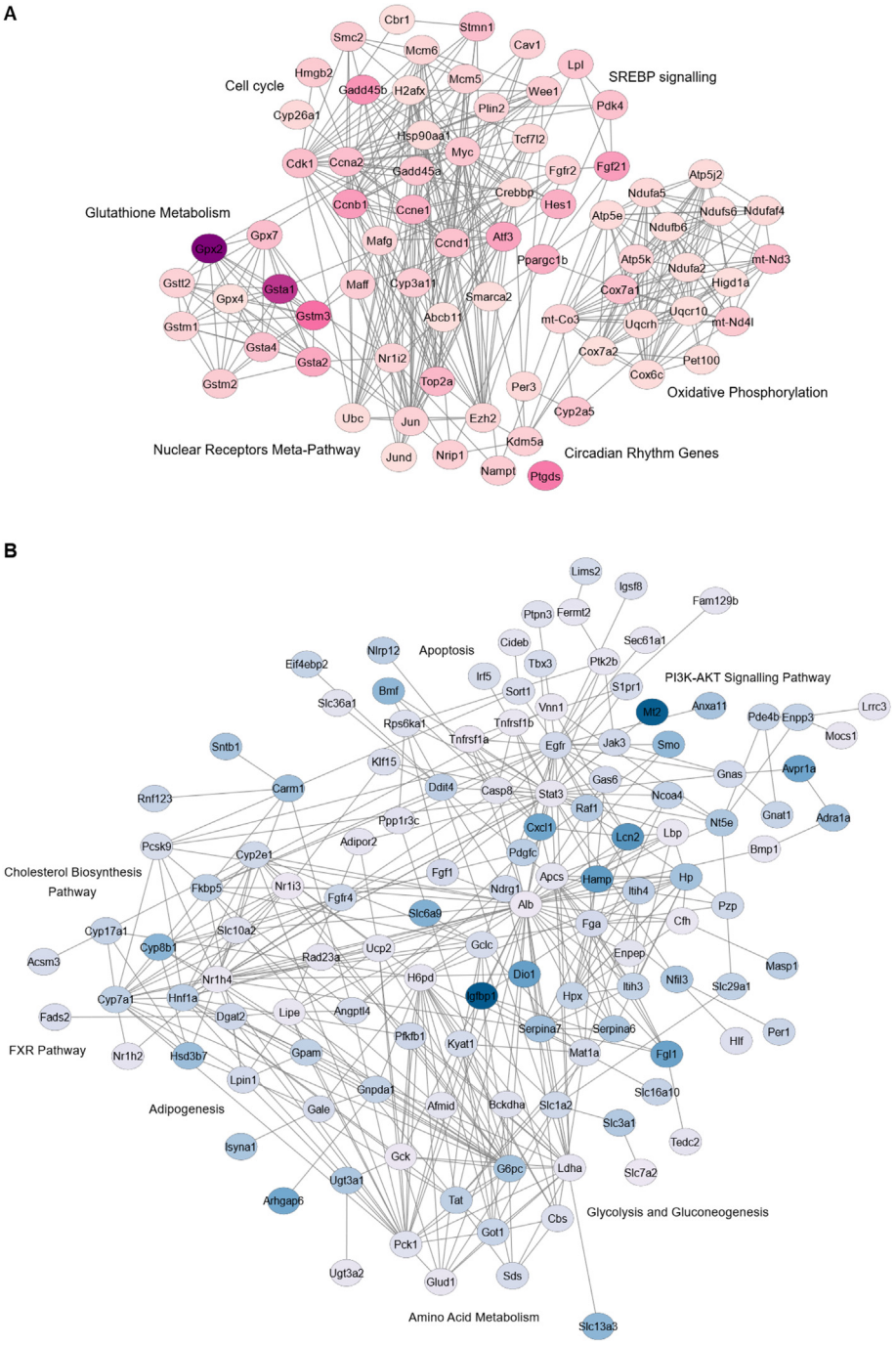

Figure 7. Contrasting differential gene expression between compound 1 and OCA. Network analysis of selected genes upregulated (**A**) and downregulated (**B**) by compound **1** in comparison to OCA. Nodes (discs) represent genes in the network and colour intensity is proportional to level of expression. Red indicates upregulated genes and blue indicates downregulated genes. Grey lines show interactions between protein products, and genes are grouped according to functional enrichment pathways, for which the main pathways are labelled. Differential expression analysis performed using DESeq2 with Wald test. Network analysis and functional enrichment of significant up- and downregulated differentially expressed genes was performed using the STRING app [56] within Cytoscape software [55] and filtered against the Wikipathway databasey [57].

FXR compared to their non-fluorinated counterparts [46]. These compounds, **1** and **2**, were highly potent and selective towards FXR, and characterisation in cell-free FRET-based assays confirmed that these compounds could induce coactivator peptide recruitment to FXR at up to 4-fold higher potencies than OCA.

Co-crystallisation of these novel compounds with human FXR LBD identified the mechanistic basis for their activity. Analysis of the FXR LBD-compound **1** complex revealed similarities to the binding pose of OCA, where its steroid nucleus partially aligned with that of OCA, maintaining interactions with several of the 'classic' bile acid binding residues (Tyr361, Tyr369, His447, and Arg331) [5]. In addition, the extended side chain of **1** was associated with the flexible loop region between helices 1 and 2 (loop 1/2), and polar interactions with residues in this area led to altered conformations of the pocket entrance. Similarly, although sharing an overlapping binding site with OCA, with the alignment of the respective interacting hydroxyl groups, compound **2** also was closely associated with loop 1/2 and helix 3. Polar interactions, in addition to fluorine contacts, van der Waals, and other non-covalent interactions from the various aromatic ring systems, stabilise the extended side chain within the buried cavities of the protein and, additionally, the distal trifluoromethyl moiety occupies the secondary binding pocket, first described by Meyer et al. [64]. Occupation of this secondary pocket has been proposed to alter coactivator recruitment in a mechanism that may be responsible for the gene-specific modulating properties of ligands such as guggulsterone [64]. To identify whether engagement of helix 3 residues and occupancy of the secondary binding pocket by our novel compounds could affect coactivator recruitment, a panel of different LXXLL motif-containing peptides was used in TR-FRET coactivator recruitment assays together with the different FXR agonists.

In the assays, compounds **1** and **2** were able to induce the recruitment of several coactivator peptides with potencies 3- to 15-times higher than OCA. Further, the assays with compound **1** displayed coactivator-specific differences in the magnitudes of the FRET signal, as well as a preference for SRC2-2, not seen with OCA, indicating differences in coactivator recruitment dependent on the ligand occupying the receptor LBD. While these results certainly indicate potential selective modulation of FXR, a limitation in these biochemical FRET assays is the reliance solely on the LBD and neglect of potential DBD or heterodimer influences. Emerging structural and computational evidence from across the nuclear receptor field has highlighted the dynamic interdomain interactions and allosteric communications between LBDs, DBDs and other regions, which can influence transcriptional activation and downstream signalling of nuclear receptors [65]. It has been well established that the hinge region between the DBD and LBD grants nuclear receptors, such as Hepatocyte nuclear factor 4 alpha (HNF4α), a physical hub for interdomain signal propagation [66]. Additionally, experiments by hydrogen–deuterium exchange mass spectrometry (HDX-MS) along with fluorescence polarisation assays have demonstrated ligand-driven alterations in spectral patterns at the distally-located DBD of the Retinoic Acid Receptor Beta (RARβ) receptor, and moreover, results showed that the distinct ligands could also affect the affinity of DNA binding at the RARβ DBD [67]. Indeed, recent studies of full length FXR, employing molecular dynamics simulations have identified ligand-specificity in the induction of DBD-LBD interactions and domain rearrangement [38]. Further structural studies employing HDX-MS, have also highlighted that ligand binding to the FXR LBD can alter DNA binding at the DBD, and reciprocally, DNA binding at the DBD can enhance the stability of LBD surfaces involved in coactivator binding and heterodimerization [68]. These studies highlight the intricate and complex mechanisms of FXR receptor regulation that have not been fully accounted for by these LBD-based biochemical assays.

Nonetheless, ligand-specific modulation of full length FXR was observed in *in vivo* studies paired with RNA sequencing. Compared to control mice, single-dose treatment with **1** for 5 days, induced significant changes in the expression of genes enriched in molecular functions such as 'Transcription coregulator activity' (GO:0003712), 'Transcription *cis*-regulatory region binding' (GO:0000976) and 'Nuclear receptor binding' (GO:0016922). Additionally, biological processes such as 'Regulation of transcription by RNA polymerase II' (GO:0006357) were also enriched. Notably, these included upregulation of RIP140 and SRC family members, alongside downregulation of TRAP complex family members. OCA treatment, however, was not associated with significant changes in the *in vivo* expression of transcriptional coregulators. While gene expression changes are only a surrogate for changes in activity at a protein level, the distinct transcriptomic signature induced by compound **1** vs OCA, indeed suggests ligand-specific coregulator usage and differential transcriptional programming.

The ligand-dependent recruitment of coactivators has been well established in some nuclear receptors, such as the oestrogen receptor, and different coactivators can cooperate with nuclear receptors to regulate explicit gene patterns in a tissue-specific manner determined by tissue-specific coactivators or chromatin remodellers [69,70]. Results presented here provide the rationale that novel compounds **1** and **2**, despite the sim-

ilarities of their steroid nucleus to OCA, can regulate FXR-target genes differentially to OCA-regulated genes, by virtue of their receptor binding modes and alternative coactivator usage.

The high potencies of **1** and **2** observed in cell-free biochemical assays, also were observed in the *in vitro* regulation of FXR-target genes, with both compounds effectively upregulating SHP, FGF19, and OSTA, and downregulating CYP7A1 in a dose-dependent manner. While **1** appeared to be equipotent with OCA, in the regulation of these target genes *in vitro*, compound **2** was even more effective, possibly arising from its multiple interactions with helix 3 and more effective occupancy of the entire hydrophobic binding pocket. However, a limitation of the *in vitro* work was the exclusive use of immortalised hepatic cell lines, which may not fully recapitulate the metabolic or transport capacities of primary hepatocytes. Further work in wild-type C57BL/6J mice was employed to investigate further the pharmacokinetic properties of these compounds, as well as to better characterise their effects on gene regulation and expression in a more representative model.

Following the pharmacokinetic studies, the progression of **2** as a candidate therapeutic drug was limited due to its restricted bioavailability and short-lived tissue residency in C57BL/6J mice. Although not investigated in the present study, future work could explore the effects of intestinal-restricted compound 2, given that intestine-specific FXR activation has also been associated with clinically favourable outcomes [71]. Compound **1**, on the other hand, displayed a more favourable pharmacokinetic profile with absorption in the intestines and effects coordinated in the liver.

Daily oral treatment of mice with compound **1** at 30 mg/kg, induced significant changes in hepatic genes involved in bile acid synthesis and transport, effects which are prototypical of FXR agonism [14,16]. Moreover, RNA sequencing revealed significant compound **1**- induced differential expression of FGFR4 and genes involved in the ERK1/2 cascade, suggesting that FXR is also being activated in the intestines, resulting in the secretion and circulation of fibroblast growth factor hormones, with enterohepatic effects contributing to the repression of bile acid synthesis in the liver [15]. This could have significant impact on the bile acid pool and circulation, and whether the downstream effects of **1** are due to FXR activation or bile acid redistribution, still needs to be investigated.

OCA treatment did not significantly induce major changes to bile acid metabolism in these *in vivo* experiments, further indicating that compound **1** is a more potent FXR agonist. However, some overlapping pathways were induced by both OCA and compound **1**. These included entrainment of the circadian clock, regulated by OCA, and circadian regulation of gene expression, modulated by compound **1**. This overlap may be the result of an FXR-directed mechanistic effect, as the relationship between FXR expression and circadian regulation is documented [72]. However, whether this effect is due to direct interactions between FXR and circadian transcriptional coregulator proteins, or via crosstalk with FXR-interacting proteins, such as HNF4a or even Rev-Erbα/β (NR1D), remains unknown.

In agreement with the differential coregulator usage, OCA and compound **1** treatment modulated divergent gene pathways in wild-type mice. In addition to bile acid synthesis, compound **1** induced the downregulation of genes enriched to lipid and glucose homeostasis, and the inflammatory response; all pathways whereby FXR is known to contribute towards regulation. Compound **1**, compared to OCA, was able to significantly downregulate key genes involved in triglyceride synthesis and gluconeogenesis, while simultaneously regulating genes involved in lipoprotein scavenging and remodelling. This suggests that one divergent effect between OCA and compound **1** may be in the deposition of lipids, cholesterol and lipoproteins.

Another effect, observed in this study, was the ability of compound **1** to upregulate genes involved in glutathione metabolism, specifically glutathione transferase and peroxidases. Glutathione transferases form part of the Phase II detoxification system that conjugates electrophilic compounds with glutathione in a process that results in their elimination, and glutathione peroxidases catalyse the reduction of hydrogen peroxide to protect cells against oxidative stress [73]. Genes involved in both processes are under the regulation of the nuclear factor erythroid 2-like 2 (NRF2) transcription factor, although here NRF2 expression itself, remains unchanged with compound **1** treatment. The expression of NRF2 protein is subject to multiple levels of regulation in addition to transcription, and different pathways have been shown to regulate its release, stability and downstream signalling [74]. Previous studies have identified that OCA can upregulate NRF2 and protect against inflammation and oxidative stress in diabetic cardiomyopathy [75]. Furthermore, recent studies have demonstrated the interplay between FXR and NRF2 activation, mediated by the Wnt signalling pathway transducer, β-catenin, and its release of the p300 transcriptional coactivator protein [76]. This demonstrates the sophistication of interconnected signal transduction pathways and highlights how ligand-induced coregulator usage can have subsequent effects on receptors, which rely on the same coregulators for transactivation or repression.

Compound **1** treatment, in contrast to OCA, was associated with significant upregulation of genes involved in the cell cycle, including cyclins D1, E1, A2 and B1, and cyclin-dependent kinases, CDK1

and CDK20. Each of these cyclins is thought to play a role during the different phases of the cell cycle, however, cyclin D1, and its binding of respective CDKs and subsequent phosphorylation of downstream cascades, is considered one of the principal driving factors initiating the transition from the G1 (growth) phase to the S (DNA synthesis) phase during cell proliferation. While the expression of cyclin D1 can be affected by NRF2 signalling, there also has been shown to be a complex interaction system between cyclin D1 and various nuclear receptors, whereby, nuclear receptors both mediate the expression of cyclin D1 and can, in turn, be mediated by cyclin D1-dependent interactions with transcriptional complexes. Our results here, confirm previous studies that have demonstrated an antagonistic effect of FXR and LXR in regulating cell cycle genes, and support studies that have mechanistically shown FXR recruitment to the promoter of cyclin D1 [77,78]. The positive correlation between FXR and cyclin D1 expression is of concern because aberrant regulation of the cell cycle has been associated with tumour formation, and overexpression of cyclin D1 has been shown in several cancers. However, contrary to the results here, other studies have identified that FXR activation can lead to the downregulation of cyclin D1 resulting in cell cycle arrest, and FXR has been characterised for its tumour-suppressive properties in different types of cancerous cells [79,80]. The dichotomous effects of FXR on cell cycle regulation may depend on the type and context of the cells, the ligand used for investigation, or the complex regulatory pathways acting downstream of FXR, further highlighting the need to isolate FXR-regulated pathways.

Conclusions

The work presented here emphasises the complexities of systemic FXR activation and the ongoing challenges in selective receptor activation. Studies here suggest that compound **1** is a highly potent agonist for FXR with the ability to efficiently mediate its effects on bile acid, lipid and glucose metabolism. Despite the similarities of their cyclopentanophenanthrene backbone, compound **1** and OCA induced slight differences in receptor conformation, which ultimately lead to differential coregulator recruitment and usage, and subsequent differences in gene regulation. Further investigation is needed to fully elucidate the pharmacologic role of compound **1** and the effective dose required to drive FXR's actions towards metabolic responses as opposed to cell proliferation. However, the data here strengthens the concept of using diverse molecular scaffolds to induce distinct gene regulation, albeit with recognition of the need to fully investigate full length receptor dynamics, in addition to how selective coregulator recruitment to one receptor affects coregulator availability at other transcription complexes. Uncovering these molecular intricacies presents interesting therapeutic opportunities to target diseases that may benefit from a more limited approach to FXR-driven gene transcription.

Financial support statement

This work was funded by NZP UK Ltd. and University of Reading.

CRediT authorship contribution statement

D. Kydd-Sinclair: Writing – review & editing, Writing – original draft, Methodology, Investigation, Formal analysis. **G.L. Packer:** Writing – review & editing, Resources. **A.C. Weymouth-Wilson:** Writing – review & editing, Project administration, Conceptualization. **K.A. Watson:** Writing – review & editing, Supervision, Project administration, Methodology, Conceptualization.

DATA AVAILABILITY

Data will be made available on request.

DECLARATION OF COMPETING INTEREST

The authors declare the following financial interests/personal relationships which may be considered as potential competing interests: 'The authors declare that the novel compounds used in this work and described in the manuscript are subject to the patent application WO2020025942. This patent covers the composition, use, and/or synthesis of the compounds reported.'.

Acknowledgements

This work was joint funded by the University of Reading and NZP UK Ltd. With thanks to Dr. Charlotte Collingham for help with the tissue culture experiments and Ms. Irene Boz for carrying out the cell viability assays (School of Biological Sciences and School of Pharmacy, respectively, University of Reading, UK).

PDB ID codes

Structures in this paper correspond to pdb_00009H65 and pdb_00009H66. Authors will release the atomic coordinates and experimental data upon article publication.

Appendix A. Supplementary material

Supplementary material to this article can be found online at https://doi.org/10.1016/j.jmb.2025.169383.

Received 11 June 2025;
Accepted 7 August 2025;
Available online 11 August 2025

Keywords:
FXR;
bile acid;
agonist;
coactivator recruitment

Abbreviations:
FXR, farnesoid X receptor; OCA, obeticholic acid; RXR, retinoid X receptor; LBD, ligand binding domain; MASH, metabolic dysfunction-associated steatohepatitis; CDCA, chenodeoxycholic acid; LDL, low-density lipoprotein; HDL, high-density lipoprotein; cAMP, cyclic adenosine monophosphate; PDB, protein databank; TR-FRET, time-resolved fluorescence energy transfer; SRC, steroid receptor coactivator; DRIP, vitamin D interacting protein; RIP, nuclear receptor interacting protein; DMSO, dimethyl sulfoxide

References

[1]. Evans, R.M., Mangelsdorf, D.J., (2014). Nuclear receptors, RXR, and the big bang. *Cell* **157**, 255–266.
[2]. Huang, P., Chandra, V., Rastinejad, F., (2010). Structural overview of the nuclear receptor superfamily: insights into physiology and therapeutics. *Annu. Rev. Physiol.* **72**, 247–272.
[3]. Khorasanizadeh, S., Rastinejad, F., (2016). Visualizing the architectures and interactions of nuclear receptors. *Endocrinology* **157**, 4212–4221.
[4]. Claudel, T. et al, (2002). Bile acid-activated nuclear receptor FXR suppresses apolipoprotein A-I transcription via a negative FXR response element. *J. Clin. Invest.* **109**, 961–971.
[5]. Mi, L.J. et al, (2003). Structural basis for bile acid binding and activation of the nuclear receptor FXR. *Mol. Cell* **11**, 1093–1100.
[6]. Huang, P., Chandra, V., Rastinejad, F., (2014). Retinoic acid actions through mammalian nuclear receptors. *Chem. Rev.* **114**, 233–254.
[7]. Rastinejad, F., Huang, P., Chandra, V., Khorasanizadeh, S., (2013). Understanding nuclear receptor form and function using structural biology. *J. Mol. Endocrinol.* **51**, T1–T21.
[8]. Rastinejad, F., Ollendorff, V., Polikarpov, I., (2015). Nuclear receptor full-length architectures: confronting myth and illusion with high resolution. *Trends Biochem. Sci.* **40**, 16–24.
[9]. Bramlett, K.S., Yao, S., Burris, T.P., (2000). Correlation of farnesoid X receptor coactivator recruitment and cholesterol 7α-hydroxylase gene repression by bile acids. *Mol. Genet. Metab.* **71**, 609–615.
[10]. Savkur, R.S. et al, (2005). Ligand-dependent coactivation of the human bile acid receptor FXR by the peroxisome proliferator-activated receptor γ coactivator-1α. *J. Pharmacol. Exp. Ther.* **312**, 170–178.
[11]. Chiang, J.Y.L., (2004). Regulation of bile acid synthesis: pathways, nuclear receptors, and mechanisms. *J. Hepatol.* **40**, 539–551.
[12]. Claudel, T., Zollner, G., Wagner, M., Trauner, M., (2011). Role of nuclear receptors for bile acid metabolism, bile secretion, cholestasis, and gallstone disease. *Biochim. Biophys. Acta BBA – Mol. Basis Dis.* **1812**, 867–878.
[13]. Xiang, D. et al, (2023). The regulation of tissue-specific farnesoid X receptor on genes and diseases involved in bile acid homeostasis. *Biomed. Pharmacother.* **168**, 115606.
[14]. Goodwin, B. et al, (2000). A regulatory cascade of the nuclear receptors FXR, SHP-1, and LRH-1 represses bile acid biosynthesis. *Mol. Cell* **6**, 517–526.
[15]. Inagaki, T. et al, (2005). Fibroblast growth factor 15 functions as an enterohepatic signal to regulate bile acid homeostasis. *Cell Metab.* **2**, 217–225.
[16]. Ananthanarayanan, M., Balasubramanian, N., Makishima, M., Mangelsdorf, D.J., Suchy, F.J., (2001). Human bile salt export pump promoter is transactivated by the farnesoid X receptor/bile acid receptor. *J. Biol. Chem.* **276**, 28857–28865.
[17]. Lee, H. et al, (2006). FXR regulates organic solute transporters α and β in the adrenal gland, kidney, and intestine. *J. Lipid Res.* **47**, 201–214.
[18]. Poupon, R., (2012). Ursodeoxycholic acid and bile-acid mimetics as therapeutic agents for cholestatic liver diseases: an overview of their mechanisms of action. *Clin. Res. Hepatol. Gastroenterol.* **36**, S3–S12.
[19]. Hirschfield, G.M., Heathcote, E.J., Gershwin, M.E., (2010). Pathogenesis of cholestatic liver disease and therapeutic approaches. *Gastroenterology* **139**, 1481–1496.
[20]. Lee, F.Y., Lee, H., Hubbert, M.L., Edwards, P.A., Zhang, Y., (2006). FXR, a multipurpose nuclear receptor. *Trends Biochem. Sci.* **31** (10), 572–580. https://doi.org/10.1016/j.tibs.2006.08.002.
[21]. Wang, Y.-D., Chen, W.-D., Moore, D.D., Huang, W., (2008). FXR: a metabolic regulator and cell protector. *Cell Res.* **18**, 1087–1095.
[22]. Han, C., (2018). Update on FXR biology: promising therapeutic target?. *Int. J. Mol. Sci.* **19**, 2069.
[23]. Venetsanaki, V., Karabouta, Z., Polyzos, S.A., (2019). Farnesoid X nuclear receptor agonists for the treatment of nonalcoholic steatohepatitis. *Eur. J. Pharmacol.* **863**, 172661.
[24]. Modica, S., Moschetta, A., (2006). Nuclear bile acid receptor FXR as pharmacological target: are we there yet?. *FEBS Letters* **580**, 5492–5499.
[25]. Chávez-Tapia, N., Uribe, M., Ponciano-Rodríguez, G., Medina-Santillán, R., Méndez-Sánchez, N., (2009). New insights into the pathophysiology of nonalcoholic fatty liver disease. *Ann. Hepatol.* **8**, S9–S17.
[26]. Pellicciari, R. et al, (2002). 6α-ethyl-chenodeoxycholic acid (6-ECDCA), a potent and selective FXR agonist endowed with anticholestatic activity. *J. Med. Chem.* **45**, 3569–3572.
[27]. De Marino, S., Festa, C., Sepe, V., Zampella, A., (2019). Chemistry and pharmacology of GPBAR1 and FXR selective agonists, dual agonists, and antagonists. In:

Fiorucci, S., Distrutti, E. (Eds.), *Bile Acids and Their Receptors*, **vol. 256** Springer International Publishing, Cham, pp. 137–165.
[28]. Nevens, F. et al, (2016). A placebo-controlled trial of obeticholic acid in primary biliary cholangitis. *N. Engl. J. Med.* **375**, 631–643.
[29]. Hirschfield, G.M. et al, (2015). Efficacy of obeticholic acid in patients with primary biliary cirrhosis and inadequate response to ursodeoxycholic acid. *Gastroenterology* **148**, 751–761.e8.
[30]. Kowdley, K.V. et al, (2018). A randomized trial of obeticholic acid monotherapy in patients with primary biliary cholangitis. *Hepatology* **67**, 1890–1902.
[31]. Eaton, J.E. et al, (2020). Liver injury in patients with cholestatic liver disease treated with obeticholic acid. *Hepatology* **71**, 1511–1514.
[32]. U.S Food & Drug Administration, Ocaliva (Obeticholic acid) by Intercept Pharmaceuticals: Drug Safety Communication – Serious Liver Injury Being Observed in Patients without Cirrhosis, 2024. https://www.fda.gov/safety/medical-product-safety-information/ocaliva-obeticholic-acid-intercept-pharmaceuticals-drug-safety-communication-serious-liver-injury.
[33]. Neuschwander-Tetri, B.A. et al, (2015). Farnesoid X nuclear receptor ligand obeticholic acid for non-cirrhotic, non-alcoholic steatohepatitis (FLINT): a multicentre, randomised, placebo-controlled trial. *Lancet* **385**, 956–965.
[34]. Mudaliar, S. et al, (2013). Efficacy and safety of the farnesoid X receptor agonist obeticholic acid in patients with type 2 diabetes and nonalcoholic fatty liver disease. *Gastroenterology* **145**, 574–582.e1.
[35]. Ratziu, V. et al, (2019). REGENERATE: design of a pivotal, randomised, phase 3 study evaluating the safety and efficacy of obeticholic acid in patients with fibrosis due to nonalcoholic steatohepatitis. *Contemp. Clin. Trials* **84**, 105803.
[36]. Patel, K. et al, (2020). Cilofexor, a nonsteroidal FXR agonist, in patients with noncirrhotic NASH: a phase 2 randomized controlled trial. *Hepatology* **72**, 58–71.
[37]. Xu, J. et al, (2023). IL -31 levels correlate with pruritus in patients with cholestatic and metabolic liver diseases and is FXR responsive in NASH. *Hepatology* **77**, 20–32.
[38]. Hazarika, S. et al, (2024). Nuclear receptor interdomain communication is mediated by the hinge with ligand specificity. *J. Mol. Biol.* **436**, 168805.
[39]. Maloney, P.R. et al, (2000). Identification of a chemical tool for the orphan nuclear receptor FXR. *J. Med. Chem.* **43**, 2971–2974.
[40]. Tully, D.C. et al, (2017). Discovery of tropifexor (LJN452), a highly potent non-bile acid FXR agonist for the treatment of cholestatic liver diseases and nonalcoholic steatohepatitis (NASH). *J. Med. Chem.* **60**, 9960–9973.
[41]. Wang, H. et al, (2017). A novel intestinal-restricted FXR agonist. *Bioorg. Med. Chem. Letters* **27**, 3386–3390.
[42]. Jiang, L., (2021). Farnesoid X receptor (FXR): structures and ligands. *Comput. Struct. Biotechnol. J.*.
[43]. Heering, J. et al, (2022). Mechanistic impact of different ligand scaffolds on FXR modulation suggests avenues to selective modulators. *ACS Chem. Biol.* **17**, 3159–3168.
[44]. Downes, M. et al, (2003). A chemical, genetic, and structural analysis of the nuclear bile acid receptor FXR. *Mol Cell.* **11** (4), 1079–1092. https://doi.org/10.1016/s1097-2765(03)00104-7.
[45]. Zheng, W. et al, (2017). A novel class of natural FXR modulators with a unique mode of selective co-regulator assembly. *Chembiochem* **18**, 721–725.
[46]. A. Weymouth-Wilson, G. Packer, B. Linclau, D. Kydd-Sinclair, K.A. Watson, Fluorinated bile acid derivatives, (2020) 1–107.
[47]. Hofmann, A.F., (1999). The continuing importance of bile acids in liver and intestinal disease. *Arch. Intern. Med.* **159**, 2647.
[48]. Winn, M.D. et al, (2011). Overview of the *CCP* 4 suite and current developments. *Acta Crystallogr. D Biol. Crystallogr.* **67**, 235–242.
[49]. Adams, P.D. et al, (2010). *PHENIX* : a comprehensive Python-based system for macromolecular structure solution. *Acta Crystallogr. D Biol. Crystallogr.* **66**, 213–221.
[50]. Emsley, P., Cowtan, K., (2004). *Coot*: model-building tools for molecular graphics. *Acta Crystallogr. D Biol. Crystallogr.* **60**, 2126–2132.
[51]. Chen, V.B. et al, (2010). *MolProbity*: all-atom structure validation for macromolecular crystallography. *Acta Crystallogr. D Biol. Crystallogr.* **66**, 12–21.
[52]. McNicholas, S., Potterton, E., Wilson, K.S., Noble, M.E. M., (2011). Presenting your structures: the *CCP* 4 mg molecular-graphics software. *Acta Crystallogr. D Biol. Crystallogr.* **67**, 386–394.
[53]. Kolberg, L. et al, (2023). g:Profiler—interoperable web service for functional enrichment analysis and gene identifier mapping (2023 update). *Nucleic Acids Res.* **51**, W207–W212.
[54]. Tang, D. et al, (2023). SRplot: a free online platform for data visualization and graphing. *PLOS ONE* **18**, e0294236.
[55]. Shannon, P. et al, (2003). Cytoscape: a software environment for integrated models of biomolecular interaction networks. *Genome Res.* **13**, 2498–2504.
[56]. Doncheva, N.T., Morris, J.H., Gorodkin, J., Jensen, L.J., (2019). Cytoscape StringApp: network analysis and visualization of proteomics data. *J. Proteome Res.* **18**, 623–632.
[57]. Agrawal, A. et al, (2024). WikiPathways 2024: next generation pathway database. *Nucleic Acids Res.* **52**, D679–D689.
[58]. Livak, K.J., Schmittgen, T.D., (2001). Analysis of relative gene expression data using real-time quantitative PCR and the $2-\Delta\Delta CT$ method. *Methods* **25**, 402–408.
[59]. Pellicciari, R. et al, (2006). Back door modulation of the farnesoid X receptor: design, synthesis, and biological evaluation of a series of side chain modified chenodeoxycholic acid derivatives. *J. Med. Chem.* **49**, 4208–4215.
[60]. Renaud, J.P., Moras, D., (2000). Structural studies on nuclear receptors. *Cell. Mol. Life Sci.* **57**, 1748–1769.
[61]. Nettles, K.W., Greene, G.L., (2003). Nuclear receptor ligands and cofactor recruitment: is there a coactivator 'on deck'?. *Mol. Cell* **11**, 850–851.
[62]. Chau, M. et al, (2019). Characterization of EDP-305, a highly potent and selective farnesoid X receptor agonist, for the treatment of non-alcoholic steatohepatitis. *Int. J. Gastroenterol.* **3**, 4.
[63]. Graton, J. et al, (2012). An unexpected and significantly lower hydrogen-bond-donating capacity of fluorohydrins compared to nonfluorinated alcohols. *Angew. Chem. – Int. Ed.* **51**, 6176–6180.

[64]. Meyer, U., Costantino, G., Macchiarulo, A., Pellicciari, R., (2005). Is antagonism of *E*/*Z*-guggulsterone at the farnesoid X receptor mediated by a noncanonical binding site? A molecular modeling study. *J. Med. Chem.* **48**, 6948–6955.
[65]. Rastinejad, F., (2025). Allosteric communications between domains of nuclear receptors. *Steroids* **214**, 109551.
[66]. Rastinejad, F., (2023). The protein architecture and allosteric landscape of HNF4α. *Front. Endocrinol.* **14**, 1219092.
[67]. Chandra, V. et al, (2017). The quaternary architecture of RARβ–RXRα heterodimer facilitates domain–domain signal transmission. *Nature Commun.* **8**, 868.
[68]. Sheng, Y. et al, (2025). Structural basis for the asymmetric binding of coactivator SRC1 to FXR-RXRα and allosteric communication within the complex. *Commun. Biol.* **8**, 425.
[69]. Ozers, M.S. et al, (2005). Analysis of ligand-dependent recruitment of coactivator peptides to estrogen receptor using fluorescence polarization. *Mol. Endocrinol.* **19**, 25–34.
[70]. Thomas, A.M. et al, (2010). Genome-wide tissue-specific farnesoid X receptor binding in mouse liver and intestine. *Hepatology* **51**, 1410–1419.
[71]. Pathak, P. et al, (2018). Intestine farnesoid X receptor agonist and the gut microbiota activate G-protein bile acid receptor-1 signaling to improve metabolism. *Hepatology* **68**, 1574–1588.
[72]. Hassan, H. et al, (2022). Regulation of chromatin accessibility by the farnesoid X receptor is essential for circadian and bile acid homeostasis in vivo. *Cancers Basel* **14**, 6191.
[73]. Pei, J., Pan, X., Wei, G., Hua, Y., (2023). Research progress of glutathione peroxidase family (GPX) in redoxidation. *Front. Pharmacol.* **14**
[74]. Li, R., Jia, Z., Zhu, H., (2019). Regulation of Nrf2 signaling. *React. Oxyg. Species Apex* **8**, 312–322.
[75]. Wu, H., Liu, G., He, Y., Da, J., Xie, (2019). Obeticholic acid protects against diabetic cardiomyopathy by activation of FXR/Nrf2 signaling in db/db mice. *Eur. J. Pharmacol.* **5**
[76]. Liu, J. et al, (2023). NRF2 and FXR dual signaling pathways cooperatively regulate the effects of oleanolic acid on cholestatic liver injury. *Phytomedicine* **108**
[77]. Wigger, L. et al, (2019). System analysis of cross-talk between nuclear receptors reveals an opposite regulation of the cell cycle by LXR and FXR in human HepaRG liver cells. *PLoS One* **14**
[78]. You, W. et al, (2017). Farnesoid X receptor, a novel proto-oncogene in non-small cell lung cancer, promotes tumor growth via directly transactivating CCND1. *Sci. Rep.* **7**, 591.
[79]. Feng, Q. et al, (2021). Activation of FXR suppresses esophageal squamous cell carcinoma through antagonizing ERK1/2 signaling pathway. *Cancer Manag. Res.* **13**, 5907–5918.
[80]. Jiang, Y. et al, (2013). Farnesoid X receptor inhibits gankyrin in mouse livers and prevents development of liver cancer. *Hepatology* **57**, 1098–1106.